Study on Seismic Base Isolation of LWR Plants (Tests on Isolator Properties and Verification of Base Isolation System Effectiveness)

M. NAKAZAWA
Tokyo Electric Power Co., Tokyo, Japan
T. NAGANO
The Kansai Electric Power Co., Inc., Osaka, Japan
A. KATO
The Japan Atomic Power Co., Tokyo, Japan
T. TAKAYANAGI, H. TERAZAKI
Taisei Corp., Tokyo, Japan

1 INTRODUCTION

A joint study has been carried out for 6 years from the fiscal year of 1985 through 1990 by 10 electric power companies, 3 vendors, and 5 construction companies with the objective of establishing a design method for base isolated LWR plants.

The results of experimental study with the objectives of understanding the properties of base isolation devices and the dynamic characteristics of base isolated building, verifying the effectiveness of base isolated system are mainly discussed in this paper.

The base isolation devices of interest in this study are those of laminated natural rubber bearings combined with separately placed dampers. Types of damper selected in this study are steel bar damper and viscous shear damper. Based on the results of parametric analyses using SDOF model, a bilinear model with a first stiffness frequency of 1.0Hz(f1), and a second stiffness frequency of 0.5Hz(f2), and an yielding shear coefficient β of 0.1 was adopted as the design isolator restoring force model.

2 BASE ISOLATION ELEMENT TEST

To grasp the characteristics of base isolation devices, tests were performed on each base isolation element such as laminated rubber bearing, steel bar damper and viscous shear damper. In the trial design of a full scale base isolated plant, the rated load of laminated rubber bearing was assumed to be 500 ton. But a semi-full scale model with a rated load of 100 ton was used in the element test. Fig. 1 shows isolator element specimens. The horizontal stiffness of the laminated rubber bearing with a rated load of 100 ton was determined to be the one corresponding to a second stiffness frequency of 0.5Hz. PC steel damper was designed using five PC steel bars so as to realize the specified isolator restoring force model when it was combined with the laminated rubber bearing of 100 ton rated load. Using Pc steel bar damper, energy can be absorbed through the yielding of materials in the flexural deformation. The viscous shear damper consists of high polymer type viscous material filled in a circular container and a resisting plate placed in the viscous material. The damping force was caused by the shear resistance of viscous material filled between the bottom of container and the resisting plate. The damping force of viscous shear damper can be expressed by the following experimental equation;

$$F = 0.0042\, e^{-0.043T} \cdot A \cdot (V/d)^{0.59} \quad \ldots\ldots (1)$$

(in which, F: damping force[ton], A: area of resisting plate[cm^2], V: relative velocity[cm/sec], T: temperature[℃] and d: distance between the resisting plate and the bottom of container[cm])

From Eq.(1), the properties of viscous shear damper were designed to have similar damping capability as those of steel damper.

Static and dynamic tests were conducted to grasp the characteristics of laminated rubber bearing which supports the dead load of super-structure. The test results were shown in Fig.

2. Regarding the relationship between horizontal stiffness and horizontal displacement, a tendency in which the horizontal stiffness decreases as the horizontal displacement increases was observed in the test results. However, the amount of deviation in the stiffness form the design value was about 10%. Furthermore, it was shown that the horizontal stiffness of laminated rubber bearing was not dependent on the loading frequency. As a result, the dynamic test results were equivalent to the static test results. As for the relationship between horizontal displacement and vertical stiffness, the vertical stiffness was decreased due to a corresponding reduction of effective pressured area accompanied by an increase in the horizontal displacement. Fig. 2(c) shows the horizontal loading test results beyond the specified design displacement of 30cm. Under an axial load of 200ton(twice the rated load), the horizontal stiffness of laminated rubber bearing exhibits a fairly linear behavior until a horizontal displacement of 30cm. Fig. 2(d) shows the test results of vertical loading beyond the rated load. The laminated rubber bearing endured an axial load corresponding to several times of the rated load.

Bi-axial loading test was conducted on each of three different isolator elements shown in Fig. 1(laminated rubber bearing, steel bar damper, viscous shear damper). As the test results, the orbits of input displacement and the horizontal one-way restoring force characteristics of the three elements are shown in Fig. 3. As shown in the figure, the hysteresis curves of laminated rubber bearing were similar regardless of loading patterns. However, in the cases of steel bar damper and viscous shear damper, the effect of bi-axial loading was observed. In Fig. 4 the equivalent stiffness and amount of energy absorption of steel bar damper, and the damping force and amount of energy absorption of viscous shear damper are compared in terms of loading patterns. The effect of loading pattern on the equivalent stiffness and the amount of energy absorption was not clearly found in case of steel bar dampers. However, there is a tendency that the damping force and the amount of energy absorption decrease as the displacement amplitude increases in case of viscous shear damper. It can be considered that this tendency was caused by temperature rising of viscous material.

In the test of steel bar damper, the energy absorbed by steel bar damper was accumulated as damage, inducing a fatigue failure of steel bar damper. To see the relationship between the displacement amplitude(δ) and the number of loading cycles(Nf) up to fatigue failure, a cyclic loading test using semi-fullscale model(32mm ϕ) and small scale model(11mm ϕ) was conducted in this study. As for the semi-fullscale model, the relationship was found as shown in Fig. 5 and can be empirically expressed in the following formula;

$$\delta \cdot Nf^{0.41} = 33 \quad \cdots\cdots\cdots (2)$$

Furthermore, when the test results of small scale model were converted to those corresponding to semi-fullscale model, it was shown that the test results of small scale model were comparable to those of semi-fullscale model.

3 TEST OF BASE ISOLATION SYSTEM

A static loading test was conducted on a base isolation system consist of a laminated rubber bearing(a rated load of 100ton) and five steel bar dampers(32mm ϕ) used in the base isolation element tests focusing on the behavior as a system, the confirmation of activation performances of the devices, and the energy absorption capability of steel dampers. The test specimen is shown in Fig. 6. The test results of one-directional as well as two directional loading cases in which displacement inputs were gradually increased were shown in Fig. 7. It was found that the outer edges of hysteresis loop where the loading changes the direction became round shape due to the effect of orthogonal two directional loading. The hysteresis characteristics of isolator are shown in Fig. 8, where the design values(using the bi-linear characteristics) were also shown. The equivalent stiffness and the amount of energy absorption were in good agreement with the corresponding design values. The more the displacement amplitude increases, the more the equivalent stiffness decreases, whereas as the amount of energy absorption increases linearly as the displacement amplitude increases. The value of equivalent damping coefficient reaches its maximum at a displacement amplitude of 10cm. The some effect of orthogonal two directional loading was observed in the curve of the relationship between the equivalent damping coefficient and the displacement amplitude. Fig. 9 shows the relationship between the total energy absorption(sum of the energies in X direction and Y direction) and the number of loading cycles in case of the constant displacement

amplitude loading. The solid marks on the figure mean that at those levels of loading cycles all steel bar damper ruptured. Although there were differences in energy accumulation process depending on loading patterns, the total amount of energy absorption was approximately equal for different loading patterns.

4 THREE-DIMENSIONAL SHAKING TABLE TESTS

Shaking table tests were conducted using a tri-axial shaking table with the maximum loading capacity of 20 ton. Scaled models for bearing, i.e., laminated rubber bearings with a rated load of 4 ton, were used in the shaking table tests. The properties of dampers were proportioned from the rated load of the laminated rubber bearing used here.

To evaluate the effects of horizontal two-directional input excitation and mass eccentricities of super-structure, the shaking table tests were conducted using a rigid body super-structure model as shown in Fig. 10. Fig. 11 shows the maximum relative displacements recorded at the center of isolator layers during two input excitations, i.e., one directional and two directional inputs. The maximum displacement response was affected by orthogonal two directional input. However, the degree of this effect was different depending on input waveform and input acceleration level. Fig. 12 shows the acceleration reduction ratio of super-structure. In all the cases, the maximum acceleration responses at the center of super-structure reduced to nearly half that of input excitation. However, for the model with mass eccentricity, some amplification in acceleration was observed at the corners of the model. Floor response spectra were shown in Fig. 13. Due to the effect of eccentricity, the maximum spectral peak value of the mode with mass eccentricity is 1.5 times that of model with no eccentricity and the period corresponding to the peak was shifted.

Using a steel frame model for super-structure as shown in Fig. 14, the effectiveness of base-isolation was confirmed and the effects of multi directional input excitation including three directional input excitation were also evaluated in the shaking table tests. Fig. 15 shows the maximum acceleration profiles of the base isolated super-structure model along with those of the non isolated super-structure model when these models were subjected to artificial earthquake motions with fairly long period contents. Due to the effect of base isolation, the acceleration response was significantly reduced showing that the acceleration at the top of super-structure was not amplified comparing to that at the base. Fig. 16 shows the maximum acceleration profile in the super-structure in case of multi directional input in which El Centro earthquake motions were used as input motions. The effect of multi directional input excitation was not shown in the horizontal acceleration response. In addition to the maximum acceleration responses, Fig. 17 shows the floor response spectra. It was shown that the spectral peak values of base isolated case were less than 1/4 those of non isolated case. Furthermore, the effect of multi directional input excitation was not clearly shown in the floor response spectra.

5 CONCLUSIONS

In the tests of isolator elements and base isolation systems, the hysteresis characteristics and the energy absorption capability of isolator elements, and the response characteristics of base isolation systems subjected to horizontal two directional input excitation were obtained. As for the seismic response characteristics of a horizontally base isolated building, it was found that, in some cases, the maximum relative displacement was slightly increased due to the effect of orthogonal directional input excitations. In the tri-axial shaking table test results, the effects of orthogonal horizontal input excitation and vertical input excitation on the acceleration response were not clearly shown in the test results.

6 ACKNOWLEDGMENTS

The cooperation from the following companies and individuals was vital in carrying out these test. The authors express sincere appreciation to these companies and individuals.
Kajima Corporation; Mr. Kaoru Mizukoshi, Obayashi Corporation; Mr. Matsutarou Seki, Shimizu Corporation; Mr. Masuhiko Kobatake, Takenaka Corporation; Mr. Satoru Aizawa

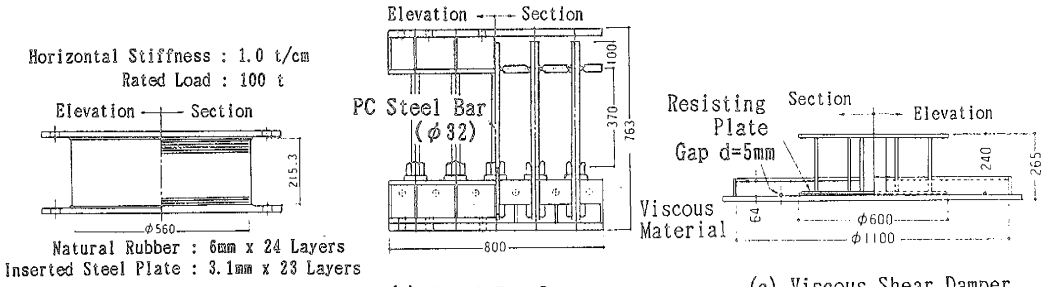

(a) Laminated Rubber Bearing (b) Steel Bar Damper (c) Viscous Shear Damper

Fig. 1 Dimensions of Base Isolation Elements

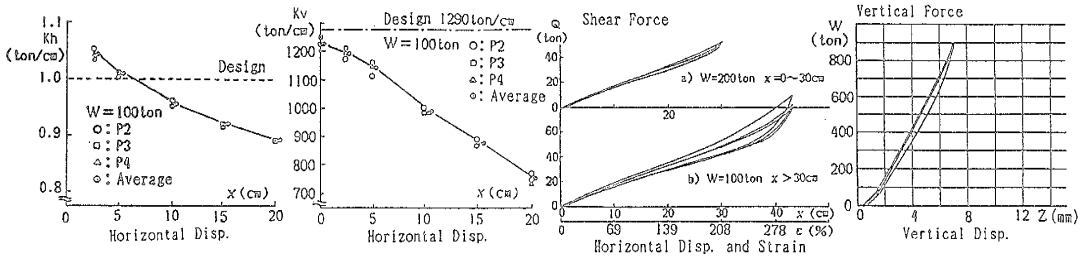

(a) Horizontal Stiffness (b) Vertical Stiffness (c) Hysteresis Loop of Horizontal Loading Test (d) Vertical Loading Test

Fig. 2 Results of Basic Characteristic Test of Laminated Rubber Bearing

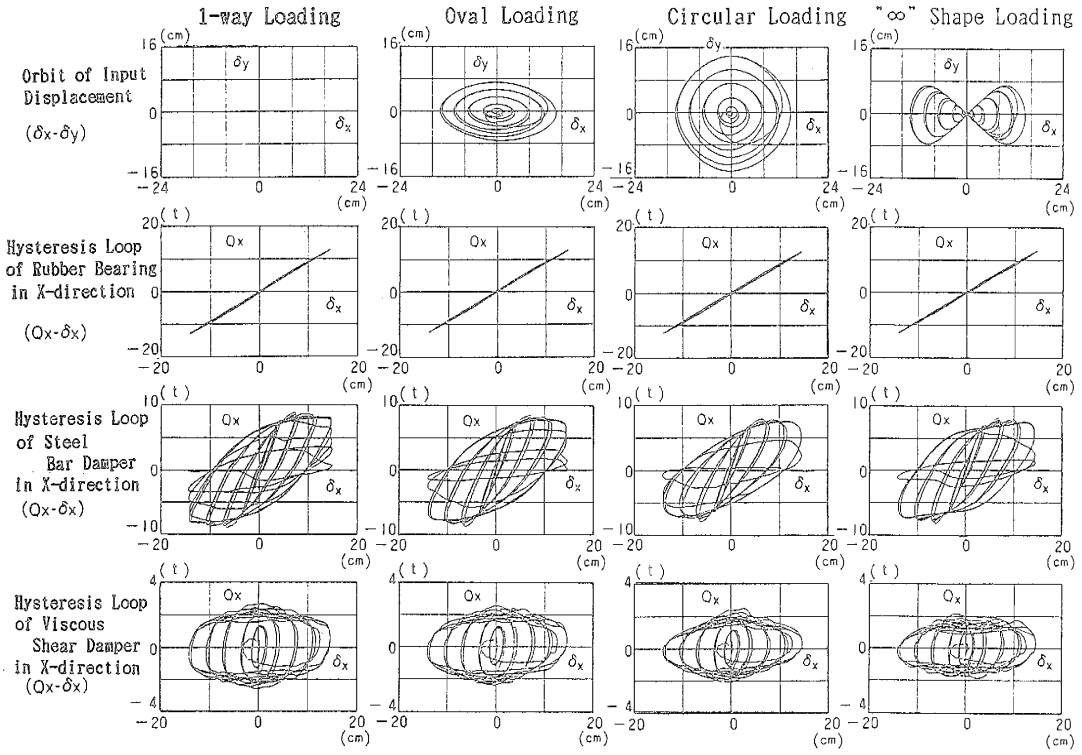

Fig. 3 Hysteresis Loops of Isolator Elements for Different Loading Patterns

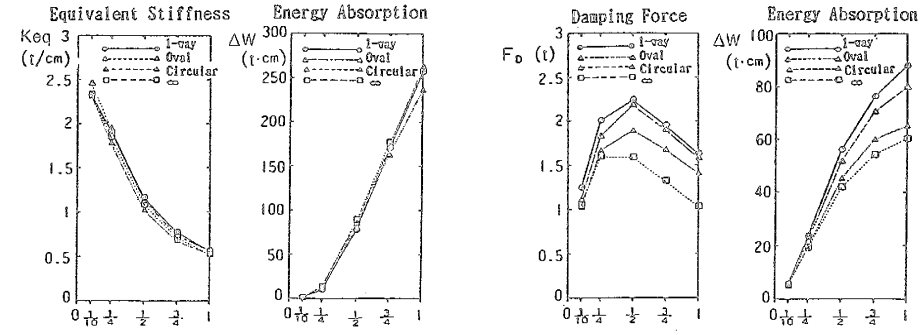

Fig. 4 Bi-axial Test Results of Dampers

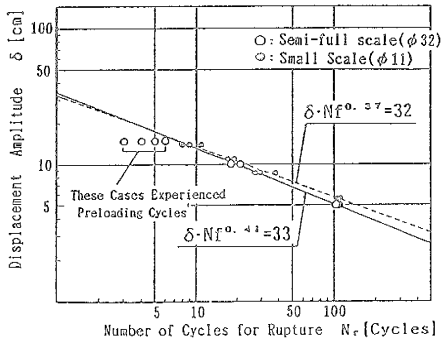

Fig. 5 Fatigue Rupture Characteristic of Steel Bar Damper

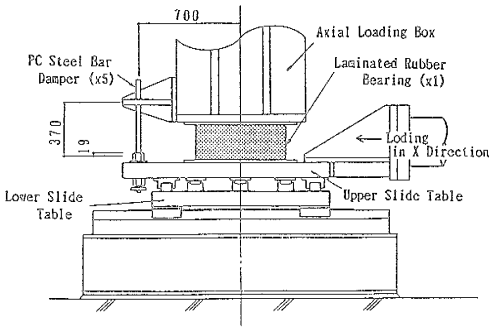

Fig. 6 Base Isolation System

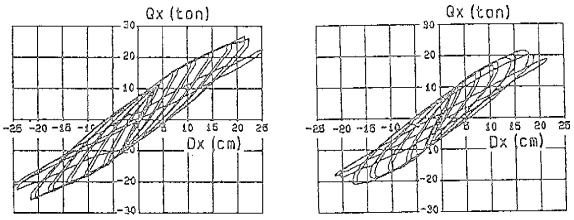

Fig. 7 Hysteresis Loop of Base Isolation System (X-direction)

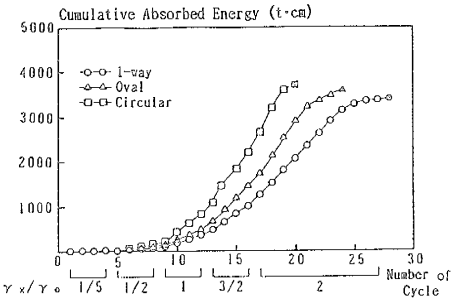

Fig. 9 Result of Repeated Loading Test

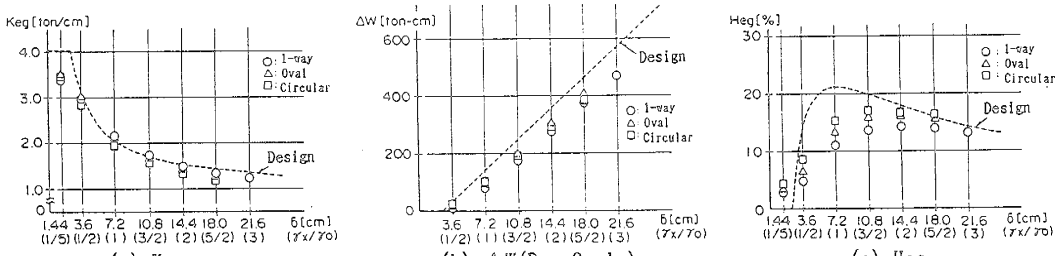

Fig. 8 Hysteresis Characteristics of Base Isolation System

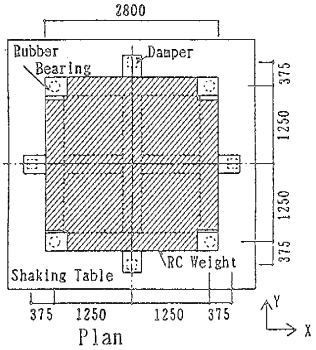

Plan

(a) No Eccentricity

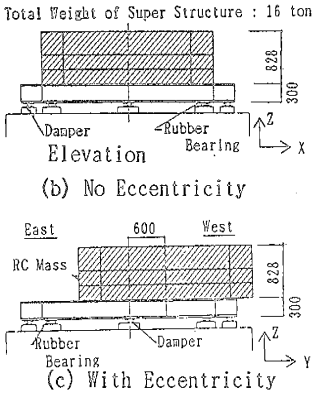

Elevation

(b) No Eccentricity

(c) With Eccentricity

Fig. 10 Rigid Body Model

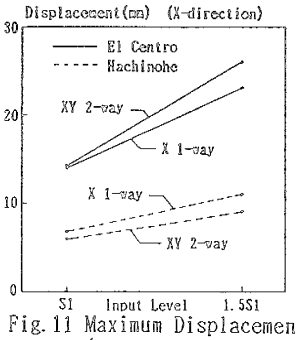

Fig. 11 Maximum Displacement (Steel Bar Damper)

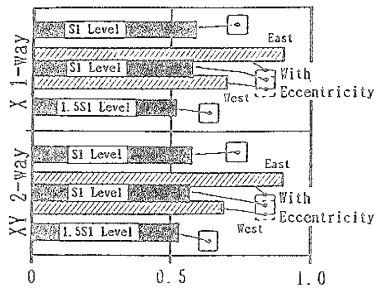

(a) Steel Bar Damper

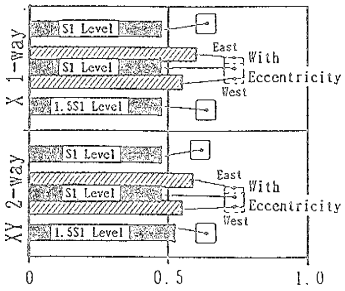

(b) Viscous Shear Damper

Fig. 12 Reduction Ratio of Acceleration (El Centro X-direction)

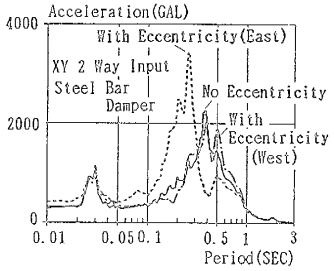

Fig. 13 Floor Response Spectra (h=1%)

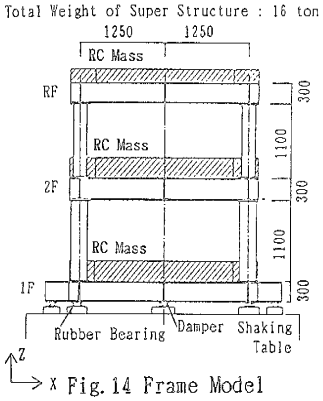

Fig. 14 Frame Model

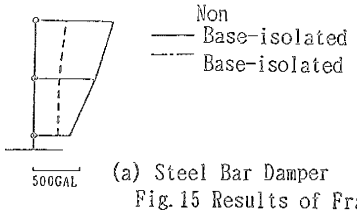

(a) Steel Bar Damper

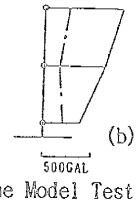

(b) Viscous Shear Damper

Fig. 15 Results of Frame Model Test

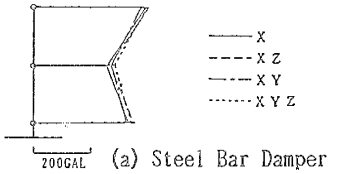

(a) Steel Bar Damper

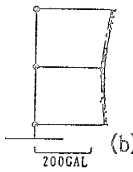

(b) Viscous Shear Damper

Fig. 16 Effect of Multi Directional Input (X-direction)

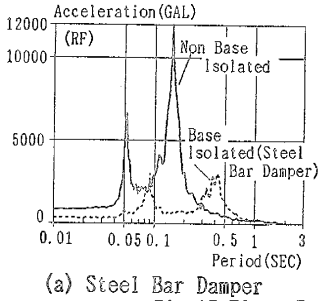

(a) Steel Bar Damper

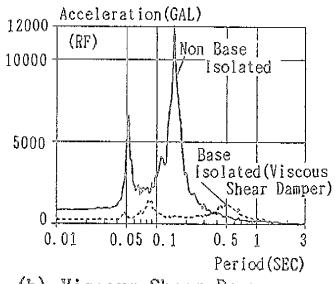

(b) Viscous Shear Damper

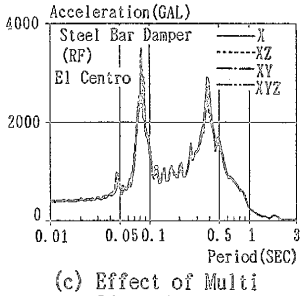

(c) Effect of Multi Directional Input

Fig. 17 Floor Response Spectra (h=1%)